

Towards Coordinated Robot Motions: End-to-End Learning of Motion Policies on Transform Trees

M. Asif Rana^{*1,3}, Anqi Li^{*2,3}, Dieter Fox^{2,3}, Sonia Chernova¹, Byron Boots^{2,3}, and Nathan Ratliff³

Abstract—Robotic tasks often require generation of motions that satisfy multiple motion constraints, that may live on different parts of a robot’s body. In this paper, we address the challenge of learning motion policies to generate motions for execution of such tasks. Additionally, to encode multiple motion constraints and their synergies, we enforce structure in our motion policy. Specifically, the structure results from decomposing a motion policy into multiple subtask policies, whereby each subtask policy dictates a particular subtask behavior. By learning the subtask policies together in an end-to-end fashion, our formulation not only learns coordination between subtask behaviors, but also learns how to trade them off against default behaviors that may exist. Furthermore, due to our choice of parameterization for the constituting subtask policies, our overall structured motion policy is guaranteed to generate stable motions. To corroborate our theory, we also present qualitative and quantitative evaluations on multiple robotic tasks.

I. INTRODUCTION

Execution of complex robotic tasks often requires simultaneous and coordinated execution of several *subtasks*, with each subtask possibly assigned to a specific robot body part. For example, imagine a sweeping task, where the robot’s elbow has to remain upright while its end-effector executes motions parallel to the surface being swept, all while avoiding collisions. Recent work on policy synthesis [1] introduced a structured motion policy class to conveniently specify such tasks. However, the problem of learning such task specifications directly from data has not been sufficiently addressed in literature. In this paper, we present an end-to-end learning approach for learning structured motion policies associated with coordinated execution of multiple subtasks.

Learning from demonstration (LfD) [2], [3] has proven to be an effective tool for learning task specifications that otherwise may be infeasible or hard to hand-code. Although there exist several techniques for learning task specifications [4]–[12], a widely used formulation involves stable (time-invariant) motion policies [13]–[16]. Compared to other methods, motion policies are known to be more robust against spatio-temporal perturbations, while the added stability property guarantees that the motions stay within a desired region of state space. However, most existing approaches [13]–[16] for learning stable motion policies, are limited to learning task specifications consisting of only a single subtask, often associated with the robot’s end-effector. Certain tasks may have multiple motion constraints,

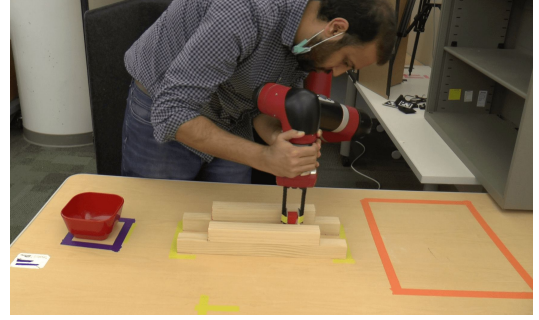


Fig. 1: A human *simultaneously* guiding multiple parts of a robot to execute a constrained manipulation task ending a goal (red bowl).

potentially on several robot body parts, and thus can be viewed as a composition of multiple subtasks.

Similar to [1], we employ a structured motion policy class to represent task specifications, parameterized by a weighted combination of several subtask policies. A subtask policy in [1], made up of an acceleration policy and a matrix weight function (i.e. a *virtual* inertia matrix), represents motion constraints associated with a specific robot body part. The inertia matrix dictates the relative influence of each subtask policy in the combination. The combined structured motion policy, along with its constituents, however was hand-specified in [1]. In this paper, we instead seek to learn this structured motion policy from expert demonstrations. While all the constituting subtask policies can be learned, one may also choose to hand-specify a subset of them. In the latter case, the overall structured policy can viewed as made up of several parameters, some of which are fixed while others learned. Thus, the structured motion policy provides additional flexibility of embedding pre-specified behaviors (e.g. obstacle avoidance) in the learning formulation.

There have been several attempts to learning the aforementioned structured motion policies [17], [18]. The formulation in [17] learns the subtask policies independently, and thus may not account for the synergies between subtasks. We contend that a principled way towards learning such structured motion policies should learn the constituting subtask policies together, in an end-to-end fashion. In this paper, we show that by training the subtask policies together, we not only learn their correct relative influences, but also learn how to trade off their influences against hand-specified subtask policies. The formulation in [18] proposes an end-to-end learning framework, but is limited to rather simple subtask policies. In this paper, we instead employ an expressive formulation of subtask policies, capable of encoding a wide range of motions. To make the resulting structured policy

* Indicates equal contribution

¹ Georgia Institute of Technology

² University of Washington

³ NVIDIA Research

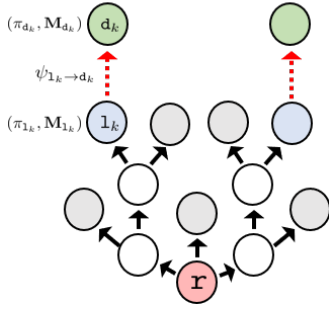


Fig. 2: A transform tree with root in the configuration space alongside hand-specified subtask/leaf nodes (grey) and learned subtask nodes (blue). Each learned subtask node is linked to a latent subtask node (green) under a chained map $\psi_{1_k \rightarrow d_k} = \psi_1 \circ \dots \circ \psi_M$.

more amenable for learning, we reformulate the structured policy class introduced in [1] in terms of velocity-based motion policies. As a part of this reformulation, we also introduce a recursive policy synthesis algorithm that efficiently combines the velocity-based subtask policies. Finally, we show that, under a particular choice of subtask policy class, our structured motion policy formulation guarantees stable robot motions.

In summary, we introduce an end-to-end motion policy learning technique that: (i) learns motions for simultaneous and coordinated execution of multiple subtasks, and (ii) guarantees the motions to be stable and kinematically feasible. We demonstrate the effectiveness of our learning approach on multiple robotic tasks that enforce motion constraints on several robot body parts.

II. MOTION GENERATION WITH TRANSFORM TREES

We are interested in learning policies on a decomposed task space given demonstrations in the robot configuration space. Before presenting our learning algorithm in Section III, we briefly introduce the motion generation problem, which can be viewed as the dual of the learning problem.

The goal of motion generation is to provide a configuration space trajectory given the desired behaviors on the task space. The robot can be tasked with multiple specifications simultaneously, which we call *subtasks*. For example, consider the task of placing an object on a shelf. The end-effector of the robot needs to reach a goal location, while also converging towards a certain approach angle. This requires coordinated movement of multiple robot body parts, each executing a subtask. Additional subtasks may also be assigned to a body part, e.g. obstacle avoidance, joint limit avoidance, or some other default behavior. A subtask can sometimes be more easily specified on its individual space, rather than the joint configuration space. For example, collision avoidance can be described as a behavior on the 1-dimensional signed distance field. This yields a motion generation problem with subtasks defined on different *subtask spaces*.

In this section, we introduce a structure for describing the overall combined task proposed in the literature [1], [19], called a *transform tree*, as well as a computational framework for motion generation with transform trees.

A. Transform trees

Consider a robot with its configuration space \mathcal{C} given by a smooth d -dimensional manifold. We assume that the configuration space \mathcal{C} admits global coordinates, called *generalized coordinates*, denoted $\mathbf{q} \in \mathbb{R}^d$. An example of generalized coordinates is the joint angles for a robot manipulator.

We assume that the overall task can be decomposed as a set of K *subtasks* defined on different *subtask spaces*, denoted $\{\mathcal{T}_k\}_{k=1}^K$. Although the maps from the configuration space \mathcal{C} to each subtask space $\{\mathcal{T}_k\}_{k=1}^K$ can be viewed as independent, we consider a more general case where there is a tree structure relating the configuration space to the subtask spaces. Such a structure exists for robotic systems, e.g. those with kinematic tree structures [20]. The tree-structure can lend itself amenable to computationally efficient algorithms through reusing computations [1].

We use a *transform tree* [1] (see e.g. Fig. 2) to describe the tree-structured map from the configuration space to subtask spaces. Each node u along the transform tree is associated with a manifold \mathcal{M} , each edge e_j corresponds to a smooth map $\psi_{e_j} := \psi_{u \rightarrow v_j}$ from the parent node manifold to the manifold associated with child node v_j . The root node in the transform tree, r , corresponds to the configuration space \mathcal{C} , and the leaf nodes $\{1_k\}_{k=1}^K$ are associated with subtask spaces $\{\mathcal{T}_k\}_{k=1}^K$. We will slightly abuse the notation to denote each subtask by its associated leaf node, e.g. subtask 1_k .

B. Policy composition on transform trees

We introduce a computational framework for motion generation on transform trees, inspired by RMPflow [1]. In contrast to RMPflow, which considers acceleration policies, we are interested instead in encoding motion as a feedback velocity policy, i.e. $\dot{\mathbf{q}} = \pi(\mathbf{q})$. To make such a policy executable, we assume that the generalized velocity $\dot{\mathbf{q}}$ can be directly controlled. For robotic systems where this does not hold, such as torque-controlled robot manipulators, a low-level tracking controller [20] can be used in conjunction with the generated policy.

Consider a subtask 1_k with a n -dimensional subtask space \mathcal{T}_k with generalized coordinates \mathbf{z}_k . We describe the *subtask policy* by a tuple $(\pi_{1_k}, \mathbf{M}_{1_k})$, consisting of a nominal velocity policy $\pi_{1_k} : \mathbb{R}^n \rightarrow \mathbb{R}^n$ along with a state-dependent matrix-valued importance weight, called the *inertia*, $\mathbf{M}_{1_k} : \mathbb{R}^n \rightarrow \mathbb{R}_{++}^{n \times n}$. The inertia matrix $\mathbf{M}_{1_k}(\mathbf{z}_k)$ denotes the directional importance of the velocity policy $\pi_{1_k}(\mathbf{z}_k)$ at point \mathbf{z}_k . For computational convenience, we also define the *momentum* policy as $\mathbf{p}_{1_k} := \mathbf{M}_{1_k} \pi_{1_k}$. Given the momentum \mathbf{p}_{1_k} and the inertia \mathbf{M}_{1_k} , the velocity policy π_{1_k} can be uniquely recovered as \mathbf{M}_{1_k} is positive definite. It should be noted that the inertia matrix \mathbf{M}_{1_k} and the momentum \mathbf{p}_{1_k} are *virtual* and do not necessarily correspond to actual physical quantities.

Given a collection of subtask policies $\{(\pi_{1_k}, \mathbf{M}_{1_k})\}_{k=1}^K$, the framework generates a *structured* configuration space velocity policy π which trades off approximation error to the policies π_{1_k} on each subtask space with an importance weight defined by the corresponding inertia matrix \mathbf{M}_{1_k} .

Formally, the policy is given by the solution to the following weighted least-squares problem:

$$\pi(\mathbf{q}; \{(\pi_{1_k}, \mathbf{M}_{1_k})\}_{k=1}^K) := \arg \min_{\mathbf{u}} \sum_{k=1}^K \left\| \pi_{1_k}(\psi_{\mathbf{r} \rightarrow 1_k}(\mathbf{q})) - \mathbf{J}_{\mathbf{r} \rightarrow 1_k}(\mathbf{q}) \mathbf{u} \right\|_{\mathbf{M}_{1_k}(\psi_{\mathbf{r} \rightarrow 1_k}(\mathbf{q}))}^2 \quad (1)$$

where $\mathbf{J}_{\mathbf{r} \rightarrow 1_k}$ is the Jacobian matrix of the subtask map $\psi_{\mathbf{r} \rightarrow 1_k}$.

Similar to RMPflow [1], we propose a computational framework for solving (1) through propagating information along the transform tree. The algorithm consists of the following four stages:

- 1) *Forward pass*: From the root node to the leaf nodes, the coordinate associated with each intermediate node is calculated based on the coordinate of its parent node: $\mathbf{y}_j = \psi_{\mathbf{e}_j}(\mathbf{x})$, where \mathbf{x} and \mathbf{y}_j are the coordinates for the parent and the child node, respectively, and $\psi_{\mathbf{e}_j}$ is the map associated with the edge. The Jacobian matrix associated with each edge, $\mathbf{J}_{\mathbf{e}_j}$, is also evaluated.
- 2) *Leaf evaluation*: For each leaf node, evaluate the momentum policy $\mathbf{p}_{1_k}(\mathbf{z}_k)$ and inertia $\mathbf{M}_{1_k}(\mathbf{z}_k)$, where the momentum policy is computed as $\mathbf{p}_{1_k}(\mathbf{z}_k) = \mathbf{M}_{1_k}(\mathbf{z}_k) \pi_{1_k}(\mathbf{z}_k)$.
- 3) *Backward pass*: From the leaf nodes to the root node, recursively compute the momentum and inertia at each node based the policies at the child nodes. Consider a node \mathbf{u} with N child nodes $\{\mathbf{v}_j\}_{j=1}^N$. The momentum and inertia at node \mathbf{u} is calculated as,
$$\mathbf{p}_{\mathbf{u}} = \sum_{j=1}^N \mathbf{J}_{\mathbf{e}_j}^\top \mathbf{p}_{\mathbf{v}_j}, \quad \mathbf{M}_{\mathbf{u}} = \sum_{j=1}^N \mathbf{J}_{\mathbf{e}_j}^\top \mathbf{M}_{\mathbf{v}_j} \mathbf{J}_{\mathbf{e}_j}, \quad (2)$$
where \mathbf{e}_j is the edge from \mathbf{u} to \mathbf{v}_j .
- 4) *Resolve*: At the root node, the velocity policy is solved as $\pi(\mathbf{q}) = \mathbf{M}_{\mathbf{r}}^{-1} \mathbf{p}_{\mathbf{r}}$.

C. Natural gradient descent systems

The configuration space motions governed by (1) exhibit several desirable properties if the leaf node velocity policies on the transform tree take the form:

$$\pi_{1_k}(\mathbf{z}_k) = -\mathbf{M}_{1_k}^{-1}(\mathbf{z}_k) \nabla_{\mathbf{z}_k} \Phi_{1_k}(\mathbf{z}_k), \quad (3)$$

where $\Phi_{1_k} : \mathbb{R}^n \rightarrow \mathbb{R}$ is called the potential function.

The system (3) can be viewed as a continuous-time version of the *natural gradient descent* system [21], which evolves along steepest descent direction of Φ_{1_k} on a Riemannian manifold defined by Riemannian metric \mathbf{M}_{1_k} . Under the assumption that each leaf node policy is given by a natural gradient descent system (3), the following properties hold for the root node policy:

- *Closure*: the motion follows natural gradient descent dynamics;
- *Stability*: the system converges to the stationary points of the function

$$\Phi_{\mathbf{r}} = \sum_{k=1}^K \Phi_{1_k} \circ \psi_{\mathbf{r} \rightarrow 1_k}. \quad (4)$$

Formally, the above properties are stated in the following theorem:

Theorem II.1. Assume that the inertia at the root node is non-singular, i.e. $\mathbf{M}_{\mathbf{r}} \succ 0$. If each leaf node policy is given by a natural gradient descent dynamical system (3), the root node policy is given by the natural descent system $\dot{\mathbf{q}} = -\mathbf{M}_{\mathbf{r}}^{-1} \nabla_{\mathbf{q}} \Phi_{\mathbf{r}}$, where $\Phi_{\mathbf{r}}$ is defined in (4). Further, if $\Phi_{\mathbf{r}}$ is proper, continuously differentiable and lower bounded, the system $\dot{\mathbf{q}} = \pi(\mathbf{q})$ converges to a forward invariant set $\mathcal{C}_{\infty} := \{\mathbf{q} : \nabla_{\mathbf{q}} \Phi_{\mathbf{r}} = 0\}$.

Proof sketch: Assume each leaf node policy is given by natural gradient descent rule, $\mathbf{p}_{1_k} = \mathbf{M}_{1_k} \pi_{1_k} = -\nabla_{\mathbf{z}_{1_k}} \Phi_{1_k}$, for all $k \in \{1, \dots, K\}$. We will prove that each node follows natural gradient descent rule: Consider any non-leaf node \mathbf{u} . Let $\{\mathbf{v}_j\}_{j=1}^N$ be the child nodes of \mathbf{u} . Suppose each child node \mathbf{v}_j follows natural gradient descent dynamics with potential $\Phi_{\mathbf{v}_j}$ and inertia $\mathbf{M}_{\mathbf{v}_j}$. At node \mathbf{u} , by (2),

$$\mathbf{p}_{\mathbf{u}} = \sum_{j=1}^N \mathbf{J}_{\mathbf{e}_j}^\top \mathbf{p}_{\mathbf{v}_j} = \sum_{j=1}^N \mathbf{J}_{\mathbf{e}_j}^\top \nabla_{\mathbf{y}_j} \Phi_{\mathbf{v}_j} = \nabla_{\mathbf{x}} \Phi_{\mathbf{u}}, \quad (5)$$

where $\Phi_{\mathbf{u}} := \sum_{j=1}^N \Phi_{\mathbf{v}_j} \circ \psi_{\mathbf{e}_j}$

Therefore, by recursively applying the analysis from the leaf nodes to the root node, we have that the root node also follows natural gradient descent dynamics $\mathbf{p}_{\mathbf{r}} = \nabla_{\mathbf{q}} \Phi_{\mathbf{r}}$. Hence, we have,

$$\frac{d}{dt} \Phi_{\mathbf{r}} = \dot{\mathbf{q}}^\top \nabla_{\mathbf{q}} \Phi_{\mathbf{r}} = -(\nabla_{\mathbf{q}} \Phi_{\mathbf{r}})^\top \mathbf{M}_{\mathbf{r}}^{-1} \nabla_{\mathbf{q}} \Phi_{\mathbf{r}} \quad (6)$$

Under the assumption $\mathbf{M}_{\mathbf{r}} \succ 0$, by LaSalle's invariance principle [22], the system converges to the forward invariant set $\mathcal{C}_{\infty} = \{\mathbf{q} : \nabla_{\mathbf{q}} \Phi_{\mathbf{r}} = 0\}$. \square

III. LEARNING STRUCTURED MOTION POLICIES

Our goal is to synthesize a *stable* configuration space policy for *simultaneous* and *coordinated* execution of multiple subtasks. The subtasks are governed by subtask policies of the form (3), some of which are learned from demonstrations. While the configuration space policy is given by (1). In this section, we provide details of our learning approach.

A. Problem statement

Let us assume the availability of N expert trajectory demonstrations in the configuration space of the robot, each composed of T_i position-velocity pairs, denoted by $\{(\tilde{\mathbf{q}}_{i,t}, \dot{\tilde{\mathbf{q}}}_{i,t})\}_{t=1}^{T_i}\}_{i=1}^N$. Let us also assume access to a transform tree with root node \mathbf{r} on the configuration space, and K leaf nodes or subtasks $\{1_k\}_{k=1}^K$. A subset of subtasks $\{1_k\}_{k=1}^{\tilde{K}}$ are learned, while the remaining $\{1_k\}_{k=\tilde{K}+1}^K$ may be hand-specified, dictating default robot behavior. A default behavior may include avoiding obstacles, avoiding joint-limits, or reaching a target with constant velocity. We also assume that the demonstrations, when mapped to subtask spaces $\{\mathcal{T}_k\}_{k=1}^{\tilde{K}}$, are directed towards a set of unique target locations $\{\mathbf{z}_k^*\}_{k=1}^{\tilde{K}}$ where \mathbf{z}_k^* is the unique target in subtask \mathcal{T}_k . With parameters θ defining the learnable subtask policies $\{(\pi_{1_k}, \mathbf{M}_{1_k})\}_{k=1}^{\tilde{K}}$, we formalize the learning problem as

$$\arg \min_{\theta} \frac{1}{\tilde{K}} \sum_{i=1}^N \frac{1}{T_i} \sum_{t=1}^{T_i} \sum_{k=1}^{\tilde{K}} \left\| \dot{\tilde{\mathbf{q}}}_{i,t} - \pi(\tilde{\mathbf{q}}_{i,t}; \theta) \right\|_{\mathbf{J}_{\mathbf{r} \rightarrow 1_k}^\top \mathbf{J}_{\mathbf{r} \rightarrow 1_k}}^2, \quad (7)$$

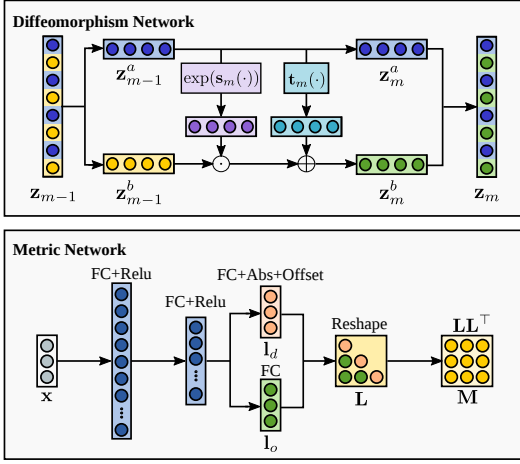


Fig. 3: *Top*: Structure of the network defining a single map ψ_m in the diffeomorphism chain [16]. *Bottom*: Structure of the network for defining latent subtask metric \mathbf{M}_{d_k} [17].

where the norm $\|\cdot\|_{\mathbf{J}_{\mathbf{r} \rightarrow \mathbf{l}_k}^\top \mathbf{J}_{\mathbf{r} \rightarrow \mathbf{l}_k}}$ maps the target and learned configuration space velocities to the subtask space \mathcal{T}_k , and penalizes their mismatch. The learned configuration space velocity $\pi(\tilde{\mathbf{q}}_{i,t}; \theta) := \pi(\tilde{\mathbf{q}}_{i,t}; \theta, \{(\pi_{1_k}, \mathbf{M}_{1_k})\}_{k=1}^K)$ is calculated by solving the weighted least-squares in (1). Note that π combines both the learned and hand-specified subtask policies. Thus, the formulation in (7) enables learned behavior to trade off against the default behavior as well. In the remainder of this section, we present an expressive class of stable learnable subtask policies which result in a stable configuration space velocity policy under Theorem II.1.

B. A class of stable subtask policies

We seek to learn a subtask policy $(\pi_{1_k}, \mathbf{M}_{1_k})$ defined on a subtask space \mathcal{T}_k with coordinates $\mathbf{z}_k \in \mathbb{R}^n$. Furthermore, we realize the velocity policy π_{1_k} by a natural gradient descent system (3) given by a potential Φ_{1_k} and an inertia matrix \mathbf{M}_{1_k} . The problem of learning a subtask policy is thus equivalent to learning a potential-inertia tuple $(\Phi_{1_k}, \mathbf{M}_{1_k})$. However, to ensure stability of the combined policy in configuration space given by (1), we impose structure in the parameterization of Φ_{1_k} and \mathbf{M}_{1_k} . Specifically, we require Φ_{1_k} to have a unique minima at a desired goal location \mathbf{z}_k^* , and \mathbf{M}_{1_k} to be always positive definite.

1) *From subtasks to latent subtasks*: Instead of explicitly parameterizing the subtask policy, we view a subtask policy in relation to another *latent* subtask policy. Specifically, we view a subtask space \mathbf{l}_k as linked under a map $\psi_{1_k \rightarrow d_k} : \mathbb{R}^n \rightarrow \mathbb{R}^n$, to a latent subtask space d_k . This results in additional edges on the transform tree (see Fig.3), each corresponding to $\psi_{1_k \rightarrow d_k}$ connecting \mathbf{l}_k to d_k . Assuming coordinates $\mathbf{x}_k \in \mathbb{R}^n$ and a natural gradient descent policy $(\Phi_{d_k}, \mathbf{M}_{d_k})$ in the latent subtask space, the relationship in (2) yields,

$$\mathbf{p}_{1_k} = \mathbf{J}_{1_k \rightarrow d_k}^\top \mathbf{p}_{d_k} = -\mathbf{J}_{1_k \rightarrow d_k}^\top \nabla_{\mathbf{y}_k} \Phi_{d_k}, \quad (8)$$

$$\mathbf{M}_{1_k} = \mathbf{J}_{1_k \rightarrow d_k}^\top \mathbf{M}_{d_k} \mathbf{J}_{1_k \rightarrow d_k} \quad (9)$$

Under a similar relationship as in (4), the subtask space motions governed by $\pi_{1_k} = \mathbf{M}_{1_k}^{-1} \mathbf{p}_{1_k}$, converge to the stationary

points of the potential function $\Phi_{1_k} = \Phi_{d_k} \circ \psi_{1_k \rightarrow d_k}$. To ensure Φ_{1_k} has a unique minima at \mathbf{z}_k^* , we impose additional constraints: (i) the latent subtask potential Φ_{d_k} has a unique minima at $\mathbf{x}_k^* = \psi_{1_k \rightarrow d_k}(\mathbf{z}_k^*)$, and (ii) the latent map $\psi_{1_k \rightarrow d_k}$ is *diffeomorphic* i.e. continuously differentiable and bijective.. Concisely, if the latent potential has a unique minima, a diffeomorphism $\psi_{1_k \rightarrow d_k}$ ensures that the resulting subtask potential also has a unique minima [16]. As shown in [16], under an appropriate choice of $\psi_{1_k \rightarrow d_k}$, the subtask potential Φ_{1_k} can generate arbitrarily curved yet stable motions, even though the latent potential Φ_{d_k} may only take a simple form. Hence, we employ a simple pre-specified latent potential, e.g. $\Phi_{d_k}(\mathbf{x}_k) = 0.5\|\mathbf{x}_k - \mathbf{x}_k^*\|^2$, and learn a diffeomorphism. The latent potential Φ_{d_k} provides stability guarantees, while the diffeomorphism $\psi_{1_k \rightarrow d_k}$ provides expressivity to the linked subtask potential Φ_{1_k} .

Furthermore, we also learn a *latent* inertia matrix \mathbf{M}_{d_k} which defines a subtask inertia matrix \mathbf{M}_{1_k} by (8). Perhaps setting $\mathbf{M}_{d_k} \equiv \mathbf{I}$ might suffice in some cases since $\psi_{1_k \rightarrow d_k}$ automatically induces a particular inertia matrix in subtask space given by its jacobian inner product. However, it should be noted that \mathbf{M}_{1_k} plays a dual role in our formulation. Specifically, the inertia matrix \mathbf{M}_{1_k} not just defines the subtask velocity policy under (3), but also acts as a priority weight associated with it during policy synthesis given by (1). Hence, we empower \mathbf{M}_{1_k} to correctly encode the synergies between subtasks, by also parameterizing the linked latent inertia \mathbf{M}_{d_k} . In the proceeding subsections, we provide details of the diffeomorphism and inertia matrix parameterizations employed in this work.

2) *A chain of diffeomorphisms*: To realize a diffeomorphism, we rely on the formulation in [16] (see Fig.3). Specifically, we view $\psi_{1_k \rightarrow d_k}$ as a chain of M simpler maps, i.e. $\psi_{1_k \rightarrow d_k} = \psi_1 \circ \dots \circ \psi_M$. Assuming coordinates $\mathbf{y}_m \in \mathbb{R}^n$ for the co-domain of ψ_m i.e. $\mathbf{y}_m = \psi_m(\mathbf{y}_{m-1})$, $\mathbf{y}_0 = \mathbf{z}_k$, and $\mathbf{y}_M = \mathbf{x}_k$, we define,

$$\mathbf{y}_m = \begin{bmatrix} \mathbf{y}_m^a \\ \mathbf{y}_m^b \end{bmatrix} = \begin{bmatrix} \mathbf{y}_{m-1}^a \\ \mathbf{y}_{m-1}^b \odot \exp(s_m(\mathbf{y}_{m-1}^a)) + t_m(\mathbf{y}_{m-1}^a) \end{bmatrix}, \quad (10)$$

where \odot and \exp denote pointwise product and pointwise exponential respectively. The components $\mathbf{y}_{m-1}^a \in \mathbb{R}^{\lfloor n/2 \rfloor}$ and $\mathbf{y}_{m-1}^b \in \mathbb{R}^{\lceil n/2 \rceil}$ constitute alternate input dimensions, with the pattern of alternation reversed after each mapping in the chain. Furthermore, $s_m : \mathbb{R}^{\lfloor n/2 \rfloor} \rightarrow \mathbb{R}^{\lceil n/2 \rceil}$ and $t_m : \mathbb{R}^{\lfloor n/2 \rfloor} \rightarrow \mathbb{R}^{\lceil n/2 \rceil}$ are learnable scaling and translation functions, respectively. We parameterize the scaling and translation functions as linear combinations of random Fourier features (10) i.e. $s_m(\cdot) := s_m(\cdot; \theta_{s_m}) = \varphi(\cdot)^\top \theta_{s_m}$, and $t_m(\cdot) := t_m(\cdot; \theta_{t_m}) = \varphi(\cdot)^\top \theta_{t_m}$, where

$$\varphi(\cdot) = \sqrt{\frac{2}{D}} [\cos(\boldsymbol{\alpha}_1^\top(\cdot) + \beta_1), \dots, \cos(\boldsymbol{\alpha}_D^\top(\cdot) + \beta_D)]^\top \otimes \mathbf{I}, \quad (11)$$

is a D -dimensional Fourier feature approximation of a matrix-valued Gaussian separable kernel [23], [24], $K(\mathbf{y}, \mathbf{y}') = \exp(-\frac{\|\mathbf{y} - \mathbf{y}'\|^2}{2l^2})\mathbf{I}$ with length-scale l . Due to the choice of parameterization in (10)-(11), ψ_m is a smooth and affine bijective map, and thus a diffeomorphism.

Consequently, the chain $\psi_{1_k \rightarrow d_k}$ is a diffeomorphism with learnable parameters $\theta_{\psi_{1_k \rightarrow d_k}} := \{\theta_{s_m}, \theta_{t_m}\}_{m=1}^M$.

3) *Inertia matrix via Cholesky decomposition*: We represent a latent subtask inertia matrix \mathbf{M}_{d_k} by its Cholesky decomposition parameterized by a matrix-valued neural network (see Fig.3). This parameterization has been previously introduced in literature [17]. Concretely, we construct $\mathbf{M}_{d_k} := \mathbf{L}_{d_k} \mathbf{L}_{d_k}^\top$, where $\mathbf{L}_{d_k}(\mathbf{x}_k) \in \mathbb{R}^{n \times n}$ is a lower-triangular matrix. We parameterize the vectorized diagonal and off-diagonal entries of \mathbf{L}_{d_k} , i.e. $\mathbf{l}_d(\mathbf{x}_k; \theta_{\mathbf{l}_d}) \in \mathbb{R}^n$ and $\mathbf{l}_o(\mathbf{x}_k; \theta_{\mathbf{l}_o}) \in \mathbb{R}^{\frac{1}{2}(n^2-n)}$ respectively, as fully-connected neural networks with RELU activations. Furthermore, the networks for \mathbf{l}_o and \mathbf{l}_d share parameters for all the layers except their output layers. To ensure \mathbf{L}_{d_k} is a valid Cholesky decomposition, and consequently \mathbf{M}_{d_k} is positive definite, we require the entries of \mathbf{l}_d to be strictly positive. In lieu of this, we take the absolute value of the output linear layer of \mathbf{l}_d and add a small positive bias $\epsilon > 0$. The parameters of the latent inertia matrix \mathbf{M}_{d_k} are concisely denoted by $\theta_{\mathbf{M}_{d_k}} := \{\theta_{\mathbf{l}_d}, \theta_{\mathbf{l}_o}\}$.

In line with the aforementioned formulations, the parameters in (7) corresponding to the learnable subtask policies are thus given by $\theta := \{\theta_{\psi_{1_k \rightarrow d_k}}, \theta_{\mathbf{M}_{d_k}}\}_{k=1}^{\tilde{K}}$.

IV. EXPERIMENTAL RESULTS

We evaluated our approach on three manipulations tasks on a 7-DOF Rethink Sawyer robot with configuration space coordinates $\mathbf{q} \in \mathbb{R}^7$. Each of the tasks is decomposed into subtasks assigned to 3 robot body parts, whereby each body part is represented by a unique *control point* (see Fig. 4 for details). Given our choice of control points, the subtask policies effectively control the end-effector pose (i.e. position and orientation). However, we stress that our learning approach is not only limited to learning robot poses. In fact, one may instead, for instance, choose to learn motion policies dictating a partial pose (by removing a control point), or pose alongside the robot elbow (by adding an additional control point). Furthermore, as shown in our experiments, our framework enables learning subtask policies in combination with other pre-specified subtask policies. Accompanying video is available at: <https://youtu.be/hwcxzLnXZPQ>.

As a prelude to learning, we setup a transform tree (see Section II-A). Specifically, the tree had its root in the robot's configuration space, and leaves associated with the subtask spaces mapped by $\psi_{\mathbf{r} \rightarrow 1_k}$. To elaborate, each leaf node 1_k had a parent node associated with one of the control points, which were further linked to the root node under the robot's kinematic chain. In the absence of any learned behaviors, the robot would execute default behavior dictated by the 3 default subtask policies. The default subtask policies, governed by a convex potential and a constant inertia matrix $\mathbf{M}_{1_k} = 10\mathbf{I}$, pull the end-effector in straight-line towards a desired goal pose. Additionally, to ensure the root inertia matrix $\mathbf{M}_{\mathbf{r}}$ is always non-singular, we added a small offset $\epsilon_{\mathbf{r}} = 0.02$ to its diagonal entries.

We consider 3 tasks including *inspection*, *placing-1*, and *placing-2*. For details about the task specifications, the reader

is referred to Figs. 6–8. For each task, a human subject provided multiple configuration space demonstrations via kinesthetic teaching, i.e. 14 demonstrations for *inspection*, 9 for *placing-1*, and 12 for *placing-2*. To bias the robot's motions towards a demonstrated behavior, we added additional $\tilde{K} = 3$ leaves to the tree, whereby each new leaf also branched out from one of the control point nodes. Overall, the tree consisted of $K = 6$ leaves. We learned the subtask policies $\{(\pi_{1_k}, \mathbf{M}_{1_k})\}_{k=1}^{\tilde{K}=3}$ as per Section III, defined by a set of diffeomorphisms $\{\psi_{1_k \rightarrow d_k}\}_{k=1}^{\tilde{K}}$ and a set of latent inertia matrices $\{\mathbf{M}_{d_k}\}_{k=1}^{\tilde{K}}$. Furthermore, each diffeomorphism $\psi_{1_k \rightarrow d_k}$ was composed of $M = 10$ chained diffeomorphisms, each parameterized by $D = 200$ random Fourier features with length-scale $l = 0.45$. On the other hand, each latent inertia matrix \mathbf{M}_{d_k} had two hidden layers with 128 and 64 dimensions respectively. The optimization problem in (7) was solved with Adam optimizer [25] with a learning rate of 1×10^{-4} and weight decay 1×10^{-8} .

To evaluate the performance of our approach, we establish two baselines: (i) an *independent* learning version whereby the subtask policies are learned independently, and (ii) a *single link* learning version where just a single control point (i.e. end-effector) is chosen and the associated subtask policy is again learned independently. Fig. 4 shows example reproductions of end-effector pose trajectories under the aforementioned variants of our algorithm. Our coordinated learning approach is observed to successfully reproduce the demonstrated motions. However, the baselines either fail to reproduce the position profile or the orientations. To quantitatively evaluate the capacity of our approach to reproduce demonstrations, we employ two error metrics i.e. mean position error, and mean orientation error. We evaluate position errors in terms of Euclidean distance i.e. $error(\mathbf{p}_1, \mathbf{p}_2) = \|\mathbf{p}_1 - \mathbf{p}_2\|_2$, where \mathbf{p}_1 and \mathbf{p}_2 are adjacent (in terms of time) end-effector positions on the demonstrated and reproduced trajectory respectively. On the other hand, for orientation error we employ $error(\mathbf{o}_1, \mathbf{o}_2) = \arccos(|\mathbf{o}_1 \cdot \mathbf{o}_2|)$, where \mathbf{o}_1 and \mathbf{o}_2 are unit quaternions representing end-effector orientations. For each comparison metric, we take the mean of the errors accumulated over the duration of a trajectory. Fig. 5 reports these comparisons as box plots. For the two *placing* tasks, our approach outperforms the baselines by a significant margin. A major contributor towards this difference in performance is the existence of default subtask policies. When learned without accounting for the existing policies, the learned policies may not be able to sufficiently bias against the default behavior. Furthermore, we also observe that the independent learning version occasionally performs worse than the single link learning variant. This is perhaps because the independently learned subtask policies may conflict with each other too. This does not manifest as much in the single link case, since there is only one learned subtask policy.

Lastly, we also test the generalization performance of our approach. For this evaluation, we execute rollouts of our motion policy from 10 novel initial configurations. We

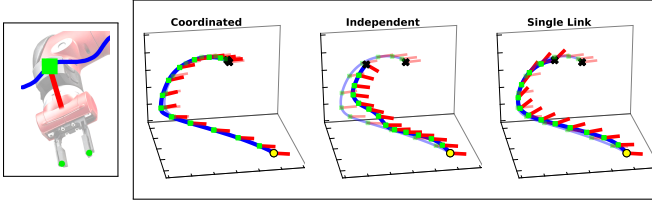


Fig. 4: *Left*: Visualization of the 3 control points (in green), with the end-effector control point denoted by a square while the two control points for gripper tips are given by circles. Overlaid is an end-effector position trajectory (in blue), and a line directed from the end-effector to the center of the gripper (in red) denoting instantaneous end-effector orientation. *Right*: Plots showing example pose trajectories starting from an initial end-effector pose (yellow circle) governed by our approach and the baselines. Also shown in the background, is the demonstration starting from the same initial pose. The final positions are denoted by black crosses.

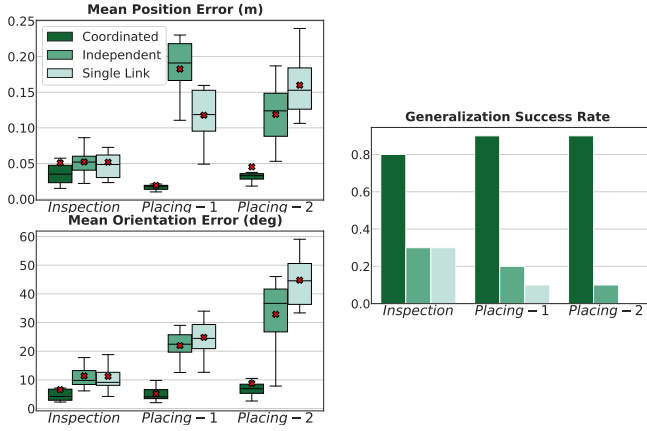


Fig. 5: Comparison of our approach against the baselines based on, mean position error (*top-left*), mean orientation error (*bottom-left*), and generalization success rate over 10 executions (*right*).

considered a rollout as successful if all the goals of the task were met without any collisions. Fig. 5(*right*) reports the success rates. Once again, our end-to-end learning approach is seen to outperform the baselines in terms of generalization success rates. We also observed that while the difference in terms of quantitative errors between our approach and the baselines was small on the *inspection* task, there were vast differences in performances given by generalization success rates. This is perhaps because, even when not trained end-to-end, the robot’s kinematic constraints may enforce certain level of coordination between subtasks, thus resulting in low reproduction errors. However, for highly constrained tasks like the ones we explore in this paper, even small errors can result in task execution failures.

Rollouts from our learned motion policies, starting from the same configurations as demonstrations, are also visualized in Figs. 6–8 (*bottom*). While we validated our approach on all the demonstrations, only a subset of rollouts is visualized here.

V. CONCLUSION

We introduced an end-to-end learning framework for learning simultaneous, coordinated and stable motions from demonstrations. The motions are governed by a structured

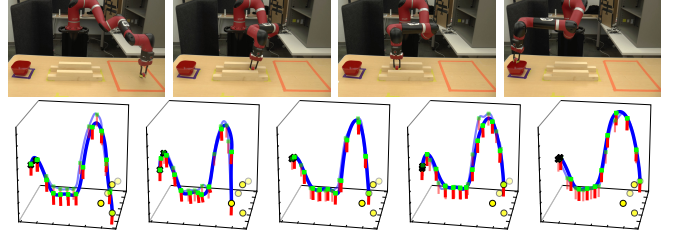


Fig. 6: The *inspection* task required the robot to pick an object from one side of the table and place it in a bowl on the other side. In the middle, the robot was required to pass a constrained pathway. *Top*: A series of snapshots showing a robot executing learned behavior. *Bottom*: Plots of a subset of motion reproductions from different initial poses, overlaid on corresponding demonstrations. The yellow circles represent the initial end-effector positions, each corresponding to one of the rollouts.

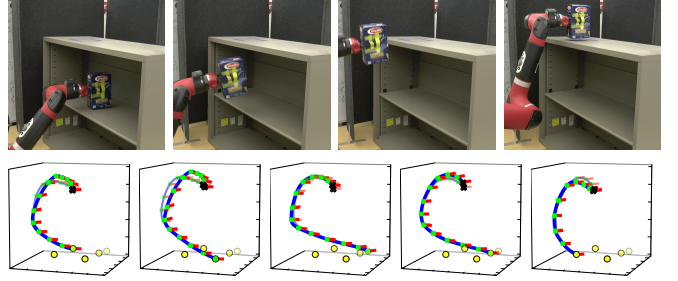


Fig. 7: The *placing-1* task required the robot pick an object from a lower shelf and place it on at a goal location on the top-most shelf at a certain orientation. *Top*: A series of snapshots showing a robot executing learned behavior. *Bottom*: Plots of a subset of motion reproductions from different initial poses, overlaid on corresponding demonstrations. The yellow circles represent the initial end-effector positions, each corresponding to one of the rollouts.

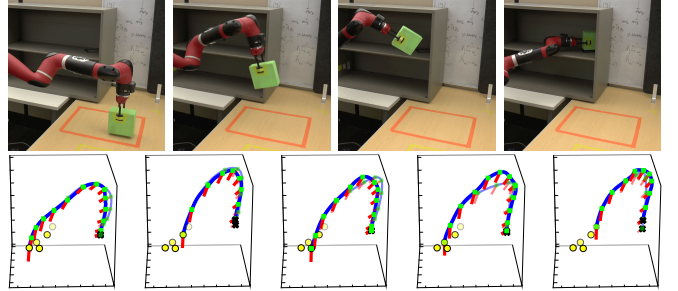


Fig. 8: The *placing-2* task required the robot pick an object from a table, significantly rotate its end-effector, and place the object on a shelf. *Top*: A series of snapshots showing a robot executing learned behavior. *Bottom*: Plots of a subset of motion reproductions from different initial poses, overlaid on corresponding demonstrations. The yellow circles represent the initial end-effector positions, each corresponding to one of the rollouts. Note that the viewing angle in the plots is different from that in the robot execution snapshots.

motion policy class, resulting from decomposing a motion policy in configuration space into several subtask policies setup on a transform tree. The underlying structure additionally allows trading off learned behaviors against pre-specified default behaviors, such that the combined behavior matches with the expert. We supplement our formulation with experiments conducted on a robot manipulator executing constrained manipulation tasks.

REFERENCES

- [1] C.-A. Cheng, M. Mukadam, J. Issac, S. Birchfield, D. Fox, B. Boots, and N. Ratliff, “RMPflow: A computational graph for automatic motion policy generation,” *Proceedings of the 13th Annual Workshop on the Algorithmic Foundations of Robotics (WAFR)*, 2018.
- [2] B. D. Argall, S. Chernova, M. Veloso, and B. Browning, “A survey of robot learning from demonstration,” *Robotics and autonomous systems*, vol. 57, no. 5, pp. 469–483, 2009.
- [3] H. Ravichandar, A. S. Polydoros, S. Chernova, and A. Billard, “Recent advances in robot learning from demonstration,” *Annual Review of Control, Robotics, and Autonomous Systems*, vol. 3, 2020.
- [4] P. Abbeel, A. Coates, and A. Y. Ng, “Autonomous helicopter aerobatics through apprenticeship learning,” *The International Journal of Robotics Research*, vol. 29, no. 13, pp. 1608–1639, 2010.
- [5] B. D. Ziebart, A. Maas, J. A. Bagnell, and A. K. Dey, “Maximum entropy inverse reinforcement learning,” 2008.
- [6] A. D. Dragan, K. Muelling, J. A. Bagnell, and S. S. Srinivasa, “Movement primitives via optimization,” in *IEEE International Conference on Robotics and Automation (ICRA)*, pp. 2339–2346, 2015.
- [7] T. Osa, A. M. G. Esfahani, R. Stolkin, R. Lioutikov, J. Peters, and G. Neumann, “Guiding trajectory optimization by demonstrated distributions,” *IEEE Robotics and Automation Letters*, vol. 2, no. 2, pp. 819–826, 2017.
- [8] H. Ravichandar, S. R. Ahmadzadeh, M. A. Rana, and S. Chernova, “Skill acquisition via automated multi-coordinate cost balancing,” in *IEEE International Conference on Robotics and Automation (ICRA)*, 2019.
- [9] S. Calinon and A. Billard, “Statistical learning by imitation of competing constraints in joint space and task space,” *Advanced Robotics*, vol. 23, no. 15, pp. 2059–2076, 2009.
- [10] A. Paraschos, R. Lioutikov, J. Peters, and G. Neumann, “Probabilistic prioritization of movement primitives,” *IEEE Robotics and Automation Letters*, vol. 2, no. 4, pp. 2294–2301, 2017.
- [11] A. J. Ijspeert, J. Nakanishi, H. Hoffmann, P. Pastor, and S. Schaal, “Dynamical movement primitives: learning attractor models for motor behaviors,” *Neural computation*, vol. 25, no. 2, pp. 328–373, 2013.
- [12] M. A. Rana, M. Mukadam, S. R. Ahmadzadeh, S. Chernova, and B. Boots, “Towards robust skill generalization: Unifying learning from demonstration and motion planning,” in *Proceedings of the 2017 Conference on Robot Learning (CoRL)*, 2017.
- [13] S. M. Khansari-Zadeh and A. Billard, “Learning stable nonlinear dynamical systems with Gaussian mixture models,” *IEEE Transactions on Robotics*, vol. 27, no. 5, pp. 943–957, 2011.
- [14] K. Neumann and J. J. Steil, “Learning robot motions with stable dynamical systems under diffeomorphic transformations,” *Robotics and Autonomous Systems*, vol. 70, pp. 1–15, 2015.
- [15] H. chaandar Ravichandar and A. Dani, “Learning position and orientation dynamics from demonstrations via contraction analysis,” *Autonomous Robots*, vol. 43, no. 4, pp. 897–912, 2019.
- [16] M. A. Rana, A. Li, D. Fox, B. Boots, F. Ramos, and N. Ratliff, “Euclideanizing flows: Diffeomorphic reduction for learning stable dynamical systems,” 2020.
- [17] M. A. Rana, A. Li, H. Ravichandar, M. Mukadam, S. Chernova, D. Fox, B. Boots, and N. Ratliff, “Learning reactive motion policies in multiple task spaces from human demonstrations,” in *Conference on Robot Learning*, pp. 1457–1468, 2020.
- [18] M. Mukadam, C.-A. Cheng, D. Fox, B. Boots, and N. Ratliff, “Riemannian motion policy fusion through learnable lyapunov function reshaping,” in *Conference on Robot Learning*, pp. 204–219, 2020.
- [19] N. D. Ratliff, J. Issac, D. Kappler, S. Birchfield, and D. Fox, “Riemannian motion policies,” *arXiv preprint arXiv:1801.02854*, 2018.
- [20] J. J. Craig, *Introduction to robotics: mechanics and control*, 3/E. Pearson Education India, 2009.
- [21] S.-I. Amari, “Natural gradient works efficiently in learning,” *Neural computation*, vol. 10, no. 2, pp. 251–276, 1998.
- [22] H. K. Khalil and J. W. Grizzle, *Nonlinear systems*, vol. 3. Prentice hall Upper Saddle River, NJ, 2002.
- [23] M. A. Alvarez, L. Rosasco, and N. D. Lawrence, “Kernels for vector-valued functions: A review,” *arXiv preprint arXiv:1106.6251*, 2011.
- [24] V. Sindhwani, M. H. Quang, and A. C. Lozano, “Scalable matrix-valued kernel learning for high-dimensional nonlinear multivariate regression and granger causality,” *arXiv preprint arXiv:1210.4792*, 2012.
- [25] D. P. Kingma and J. Ba, “Adam: A method for stochastic optimization,” *arXiv preprint arXiv:1412.6980*, 2014.